LBL--33206

DE93 010420

THEORY OF ROTATIONAL POPULATION PATTERNS IN HEAVY-ION TRANSFER REACTIONS: EVEN-EVEN THORIUM NUCLEI

S. Y. Chu, J. O. Rasmussen, R. Donangelo, M. A. Stoyer,
S. Frauendorf, and Y. R. Shimizu

Nuclear Science Division, Lawrence Berkeley Laboratory
University of California, Berkeley, California 94720, USA

November, 1992

This work was supported by the Director, Office of Energy Research, Division of Nuclear Physics of the Office of High Energy and Nuclear Physics of the U.S. Department of Energy under Contract DE-AC03-76SF00098

THEORY OF ROTATIONAL POPULATION PATTERNS IN HEAVY-ION TRANSFER REACTIONS: EVEN-EVEN THORIUM NUCLEI

S. Y. CHU and J. O. RASMUSSEN
Lawrence Berkeley Laboratory
Berkeley, CA 94720

R. DONANGELO
Universidade Federal do Rio de Janeiro
Rio de Janeiro, Brazil

M. A. STOYER
Lawrence Livermore National Laboratory
Livermore, CA 94551

S. FRAUENDORF
Institut für Kern- und Hadronenphysik, Forschungszentrum Rossendorf
PF 19, 0-8051 Dresden, Germany

and

Y. R. SHIMIZU
Physics Department, Kyushu University 33
Fukuoka 812, Japan

ABSTRACT

A Hamiltonian matrix diagonalization (HMD) method is applied to calculate the lowest several bands in ^{230,232,234}Th. Neutron pair transfer strength distributions are calculated and compared between HMD and cranked Hartree-Fock-Bogoliubov plus Random Phase Approximation (CHFB+RPA). Sudden-approximation methods are applied to estimate pair transfer population patterns in ^{206}Pb+^{232}Th reactions. Band-crossing, pairing, and spin alignment properties are also discussed.

1. Introduction

The subject of transfer reactions among heavy ions is a vast topic, and we must necessarily focus on a small niche area in this paper. We shall present neutron-pair transfer calculations among the thorium nuclei of mass 230, 232, and 234 with collision partners some of the even isotopes of Zr and Pb. The enhancement of ground-to-ground pair transfer by the pairing-force superfluidity in nuclei has long

been known[1]. The even-even ^{232}Th and its nearest neighboring isotopes are of special interest in view of the extensive studies on heavy-ion neutron transfer by groups at Heidelberg and Darmstadt[2].

The circumstances under which some pair-transfer strength also goes to excited states have been investigated, and the notion of pairing vibrational excitation is associated with this subject[3]. Much remains to be learned, despite extensive experimental and theoretical work. Theory is less reliable for excited states than for ground, since variational methods predominate in nuclear structure theory of the heavier nuclei, and variational theories tell us best about lowest energy levels of a given spin, the yrast levels.

By going to transfer between heavy nuclei, where one nucleus is deformed and has rotational bands, an extra complication (richness) enters in the form of multiple Coulomb, and nuclear, excitation on inward and outward paths of the collision. Thus, transfer near closest approach involves excited rotational states as well as ground. It has been a hope[4] that heavy-ion pair transfer might be a probe of the expected Coriolis antipairing (CAP) effect, whereby the pairing correlation diminishes steadily with increasing spin. The bandcrossing (backbending[5]) of spin-aligned[6] bands has been a complication to measuring CAP but is interesting in its own right. It is an open question whether Berry-phase interference effects can be experimentally measured by driving heavy-ion 2-neutron transfer paths through the vicinity of diabolic points, where the energy sheets in the plane of chemical potential and angular velocity touch[7].

The sharpness of band crossing is known to depend sensitively on the position of the chemical potential with respect to the Nilsson levels of the highest-j orbital[8]. The sharpest band crossings occur when the chemical potential is slightly above one of the levels with projection 3/2 through $j-1$. Quasiparticle (CHFB) methods, without RPA corrections, may have difficulty due to proximity to CHFB pairing collapse. The RPA corrections, putting in fluctuations of the pairing field, improve the situation. Very close to the band crossing CHFB+RPA still has problems, and this, coupled with the need for accurate number-conserving, and angular-momentum conserving wave functions for transfer calculations, prompted some of us to turn to exact diagonalization of the Hamiltonian matrix (HMD) in a multiparticle-plus-rotor model. The main deterrent to HMD is the explosion in the number of configurations as the number of Nilsson basis states approaches a dozen. The random-phase-approximation methods with deformed basis states and pairing force in a rotating field have the virtue that they can span a much larger space of basis states than the HMD. The RPA methods are also conceptually useful, since they allow introducing the rotation of a static deformation of the pair field and its vibrations around this mean value (dynamic pairing), exploiting the close analogy to the nuclear shape degrees of freedom[9,10].

Space limitations here do not allow a comprehensive review of developments in this area, but the 1986 review of Broglia *et al.*[9], covers developments to that time very well. Somewhat away from the point of collapse of static pairing the CHFB+RPA method is a relatively good approximation that is able to cover a realistic

single-particle space. Thus, in this paper we present and compare results from HMD and from CHFB+RPA. Engeland has reviewed Hamiltonian matrix diagonalization methods and presented results a few years ago[11]. These HMD methods have a long history, being the traditional approach to spherical shell-model structure calculations close to closed shells, or in the case of the sd shell used comprehensively with very large matrices[12]. In the case of mid-shell spheroidal nuclei, though, we have the combinatorial explosion in the number of configurations within a shell mentioned above. Half-filled systems of six equally-spaced Nilsson orbitals were studied in the 60's to gain insight on the sharpness of pairing collapse with changing pairing strength relative to level spacing[13]. Half-filled systems with two sets of degenerate levels were found to have exact solutions and furnished further understanding of critical pairing phenomena[14]. Restriction of studies to 0+ levels of deformed nuclei kept matrices at reasonable dimensions for systems of 9 Nilsson orbitals about the chemical potential and 4 or 5 pairs[15]. These matrices have the dimension of the binomial coefficient $9!/(4!\times 5!)$, which is 126. In order to reproduce high spin and bandcrossing phenomena our newer approach in the rare-earth studies was to keep the set of 9 Nilsson orbitals but to allow broken pairs in the highest-j orbital, $i_{13/2}$, projections 1/2, 3/2, and 5/2. By truncating states with $K > 2$ the dimension is 266. In contrast to Hara, Sun, and Ring's angular-momentum projected Hartree-Fock-Bogoliubov calculations[16] the aligned band does not stay intact at spins well below the crossing. The aligned-spin property appears to admix onto higher excited states, while the first excited (yrare) band takes on a pairing-vibration character at low spins. Due to the severe truncation of the basis in the HMD calculations and the constraint against broken pairs in the low j-orbitals, caution is in order regarding the pairing decrease at highest spins and about magnitude of pair-transfer enhancement. Thus, it is important to compare these properties with large-space models as we do in this paper.

The even-even ^{232}Th and its nearest neighboring isotopes are of special interest in view of the extensive studies on heavy-ion neutron transfer by groups at Heidelberg and Darmstadt[2].

For the 2n transfer calculations of this paper we choose to work within the sudden approximation (negligible nuclear rotation during the collision time) using and extending tested Classical Limit $\mathcal{S}$-matrix methods (CLSM)[17]. The CLSM sudden methods are expected to be quite valid for projectiles up to Zr and somewhat beyond, incident on actinides, with their large moments of inertia.

2. Diagonalization Calculation for the Thorium Region

We shall not give a detailed discussion of the HMD method here, since it is contained in the work of Engeland[11]. The differences with that work are as follows:

- we use 12 orbitals, rather than his 13
- we allow broken pairs in the lowest 4 of the high-j $j_{15/2}$ orbitals, rather than all of them

- the quadrupole-pairing term in our code is turned off
- the recoil energy terms are calculated only for the four lowest $j_{15/2}$ orbitals.

The truncation to omit configurations with $K > 2$ is as before. For our calculation the matrix dimension is 2646 for ^{232}Th, with 12 active neutrons, and 2220 for ^{234}Th and ^{230}Th, with 14 and 10 neutrons, respectively. Engeland did not deal with such large matrices but separately diagonalized submatrices of given projection K values, then did an overall diagonalization; his procedure involves some approximation compared to our handling of the very large matrices directly. We omit quadrupole pairing in order to facilitate the comparison with the earlier comprehensive structure calculations in the actinides by Egido and Ring[18] and with the CHFB+RPA calculations of Shimizu and Frauendorf[19] on thorium nuclei presented below. There seems no clean nuclear property by which to adjust the quadrupole pairing strength, and we defer study of its effects to a later time. Thus, our Hamiltonian simplifies to

$$\mathbf{H} = \sum_{\nu} \epsilon_{\nu}\, \mathbf{a}^{\dagger}_{\nu}\, \mathbf{a}_{\nu} - G\, \mathbf{P}^{\dagger}\, \mathbf{P} + \mathbf{H}_{\rm rot} \tag{1}$$

where

$$\mathbf{P} = \sum_{\nu>0} \mathbf{a}_{\bar{\nu}}\, \mathbf{a}_{\nu} \tag{2}$$

$$\mathbf{H}_{\rm rot} = \frac{\hbar}{2\vartheta}\left(\mathbf{R}^2_{x'} + \mathbf{R}^2_{y'}\right) \tag{3}$$

where ν is the index for the single particle level, the ϵ_{ν} is the single particle energy, the operators $\mathbf{a}^{\dagger}_{\nu}$, and $\mathbf{a}_{\nu}$ are the particle creation and annihilation operators for level ν, G is the monopole pairing constant*, and the $\mathbf{R}$ is the rotor angular momentum and x', y', z' are the nucleus bodyfixed coordinates. Following the particles plus rotor model, the rotor angular momentum is expressed in terms of total spin $\mathbf{I}$ and the angular momentum from all the valence particles, $\mathbf{J}$, namely,

$$\mathbf{R} = \mathbf{I} - \mathbf{J} \tag{4}$$

$$\mathbf{J} = \sum_{\nu_1\nu_2} < \nu_2\,|\,\mathbf{j}\,|\,\nu_1 > \mathbf{a}^{\dagger}_{\nu_2}\mathbf{a}_{\nu_1} \tag{5}$$

and the $\mathbf{H}_{\rm rot}$ can be written as follows:

$$\mathbf{H}_{\rm rot} = \frac{\hbar}{2\vartheta}\left[\left(\mathbf{I}^2 - \mathbf{I}^2_{z'}\right) - \sum_{\nu_1\nu_2}\left(\mathbf{I}_+\,(j_-)_{\nu_2\nu_1} + \mathbf{I}_-\,(j_+)_{\nu_2\nu_1}\right)\mathbf{a}^{\dagger}_{\nu_2}\mathbf{a}_{\nu_1}\right] + \frac{\hbar}{2\vartheta}\mathbf{H}_{jj} \tag{6}$$

*Actually the pairing term in the Hamiltonian should be symmetric in order $(\mathbf{P}^{\dagger}\mathbf{P}+\mathbf{P}\mathbf{P}^{\dagger})/2$. For our ^{232}Th case, where the neutron orbital system is exactly half-filled, the results are identical. For the other systems, not half-filled, there are small differences, analogous to the usual neglect of V^4 terms in the CHFB formulations. By inserting a sum over complete set of states between operators, *i.e.*$(\mathbf{P}^{\dagger}\,|\,A-2,\alpha><A-2,\alpha\,|\,\mathbf{P}+\mathbf{P}\,|\,A+2,\alpha><A+2,\alpha\,|\,\mathbf{P}^{\dagger})/2$ one gets a sum rule on pair transfer strengths in relation to our calculated expectation values and off-diagonal elements of the pairing term in the Hamiltonian.

where

$$(j_\pm)_{\nu_2\nu_1} \equiv < \nu_2 \,|\, \mathrm{j}_\pm \,|\, \nu_1 > \equiv < \nu_2 \,|\, \mathrm{j}_{x'} \pm i\, \mathrm{j}_{y'} \,|\, \nu_1 > \tag{7}$$

$$\begin{aligned} \mathbf{H}_{jj} = & \frac{1}{2} \sum_{\nu_1 \nu_2} \left[\sum_{\nu} \left((j_+)_{\nu_2 \nu} (j_-)_{\nu \nu_1} + (j_+)_{\nu \nu_1} (j_-)_{\nu_2 \nu} \right) \right] \mathbf{a}^\dagger_{\nu_2} \mathbf{a}_{\nu_1} \\ & - \sum_{\substack{\nu_1 < \nu_2 \\ \nu_3 < \nu_4}} \left(\begin{array}{c} (j_+)_{\nu_3 \nu_2} (j_-)_{\nu_4 \nu_1} - (j_+)_{\nu_4 \nu_2} (j_-)_{\nu_3 \nu_1} \\ + (j_+)_{\nu_4 \nu_1} (j_-)_{\nu_3 \nu_2} - (j_+)_{\nu_3 \nu_1} (j_-)_{\nu_4 \nu_2} \end{array} \right) \mathbf{a}^\dagger_{\nu_3} \mathbf{a}^\dagger_{\nu_4} \mathbf{a}_{\nu_2} \mathbf{a}_{\nu_1} \end{aligned} \tag{8}$$

Matrix diagonalization is done with the code using the Lanczos algorithm[20], and we calculate only the lowest eight eigenvalues and eigenvectors. Table 1 lists the neutron single-particle energies used both in our HMD and CHFB+RPA calculations. These energies are from Bengtsson and Ragnarsson[21]. The strength parameter G for pairing needs to be renormalized to larger than the values used in traditional CHFB calculations with two oscillator shells of orbitals active, since we have 12 orbitals in all. Since there is no gap parameter Δ in our calculation, we take the

Table 1. Relative neutron single-particle energy (MeV)

$\Omega^\pm$	B & R*	Bunched	Nazarewicz×
$1/2^{-\dagger}$	−1.8460	−1.8460	−0.8951‡
$3/2^{-\dagger}$	−1.0882	−1.0882	−0.5900‡
$5/2^{-\dagger}$	0	0	0‡
$7/2^{-\dagger}$	1.2276	1.2276	1.1230‡
$5/2^-$			−1.1918
$1/2^-$	−0.8881	−0.05	
$3/2^+$	−0.7413	−0.02	−0.2638‡
$5/2^+$	−0.3465	0.02	0.1354‡
$1/2^+$	0.4754	1.20	0.8934‡
$5/2^+$	0.6964	1.25	1.3288‡
$7/2^+$	1.1440	1.27	1.8730‡
$1/2^-$	1.9430	1.9430	
$9/2^-$			2.3461
$7/2^+$	1.9917	1.9917	2.5776

Table 2. Relative proton single-particle energy (MeV)

$\Omega^\pm$	Nazarewicz
$1/2^{+\dagger}$	−0.5338
$3/2^{+\dagger}$	0
$5/2^{+\dagger}$	1.1435
$3/2^+$	−1.0881
$3/2^-$	−0.9501
$1/2^+$	−0.8561
$1/2^-$	−0.5047
$5/2^-$	1.2051
$3/2^-$	1.7363

† These are $i_{13/2}$ orbitals.

† These are $j_{15/2}$ orbitals.

‡ These neutron orbitals also used in grand combined calculations.

* Bengtsson & Ragnarsson[21] for deformation $\epsilon_2 = 0.2$ and $\epsilon = -.056$

× Nazarewicz code SWGAMMA for deformation $\beta_2 = .208$ and $\beta_4 = .105$, see Sec.8

expectation value $< 0 \mid \mathbf{P}^\dagger \mathbf{P} \mid 0 >$ for the ground state. It can be shown for the ground state that the product of G times the square root of this expectation value roughly corresponds to Δ, the odd-even mass difference. The rotor moment-of-inertia is taken as constant and adjusted separately for each of the three thorium nuclei so that the energy of the 12+ state of each is correct. As the non-linear region of proton alignment is reached, the neutron calculation will be subject to corrections. In the theoretical calculation of reference[18] the onset of proton alignment in the thoriums is rather abrupt, occurring around spin 24, so the neutron-only calculation should be valid below this spin. However, since Egido and Ring had a different Hamiltonian than Bengtsson and Ragnarsson[21], the alignment behavior could well be due to small differences in single-particle level energies.

Figs.1-3 show results of the HMD method for ^{230,232,234}Th, respectively. The insets *a* (upper left) give the lowest eight energy values as a function of spin. Insets *b* (upper right) are traditional backbending plots for the yrast levels, using the so-called kinematic moment-of-inertia[1] J. Insets *c* (lower left) are the expectation values of the monopole pairing operator for yrast (×), yrare (+), and the off-diagonal value (-) connecting the two. Finally, insets *d* are shown the aligned angular momenta, which are calculated as the expectation value $< I\alpha \mid \mathbf{I} \cdot \mathbf{J} \mid I\alpha > / \sqrt{I(I+1)}$, where **J** is define in Eq.5, and α designates the additional quantum numbers required to uniquely label the eigenstate. The aligned angular momenta are shown for yrast (×) and yrare (+). For none of these three nuclei is there a sharp band crossing between yrast and yrare, consistent with what is experimentally known. In contrast the work of Egido and Ring[18] shows an abrupt neutron alignment in ^{230}Th, where the chemical potential lies just above the $j_{15/2}$ 5/2− orbital. It is important to point out that the sharpness of band crossing is very sensitive to the Nilsson-level energies near the chemical potential. Our calculations (not shown here for lack of space) using single-particle Nilsson energies calculated from a program of Nazarewicz do show sharp band crossing in ^{230}Th due to neutron alignment, but our huge-space calculations using both broken proton and neutron pairs in coupled mode, to be discussed later, show a soft bandcrossing, despite the use of the same Nazarewicz-code neutron energies. Thus, agreement with experiment on sharpness of backbending is not a very fundamental test of a given theoretical approach or model; sharpness of band crossing can be "tuned" in or out merely by shifting one level near the Fermi surface.

In all cases (Figs.1*c*, 2*c*, and 3*c*) the ground band shows a Coriolis antipairing effect. The first excited band shows a reduced pairing correlation at low spins and cross-over effects near crossing spins around 18-20. The corresponding d parts of the figures show at lowest spins alignment of the $j_{15/2}$ orbitals that at first go linearly with spins, the yrare band always showing more alignment than the yrast. This linear alignment region is where the $j_{15/2}$ contributes simply to renormalized the moment-of-inertia. At higher spins the alignment is non-linear and will be manifested in rotational energy correction terms to the normal $I(I+1)$ spacing. The linear alignment slope of the yrare band is always more than that of the yrast band. This

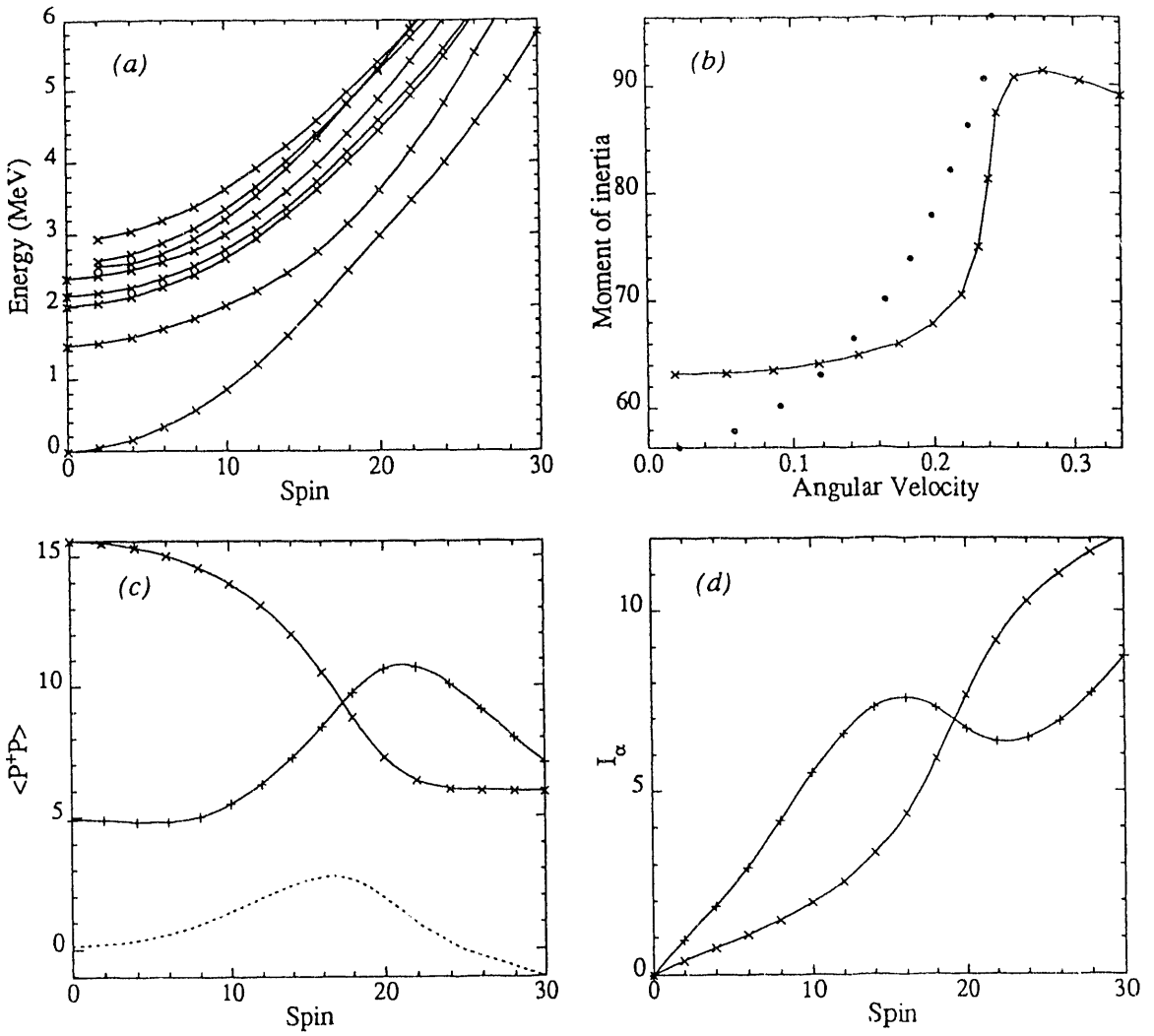

Figure 1: Result of HMD calculations using 12 Nilsson neutron levels with Bengtsson-Ragnarsson energies[21] (*a*) HMD energies for the yrast and lowest seven even-parity neutron-excitation bands in ^{230}Th. (*b*) Traditional yrast "backbending" plot, kinetic moment-of-inertia *vs.* angular velocity (MeV) (the dots are experimental values). (*c*) Expectation values of the pairing-operator for yrast(×) and yrare (+) states. The dashed line is the off-diagonal value of the pairing operator, and it is a measure of pairing vibration strength in the yrare state. There is evidently very little pairing vibration strength in the ^{230}Th yrare band. (*d*) neutron spin alignment for yrare and yrast bands.

greater contribution to moment-of-inertia and the reduced pairing correlation in the low-spin yrare states can be trivially understood as characteristics of states with components of two-quasiparticle $K = 0$ excitation of the correlated ground state. That the three thorium isotopes shown here have a good deal of similarity, except for the sharper upbending and simpler crossing phenomena in ^{230}Th, is a consequence of a rather uniform single-particle level spacing in the Bengtsson and Ragnarsson level set of Table 1. Other single-particle level schemes tend to show a neutron subshell at

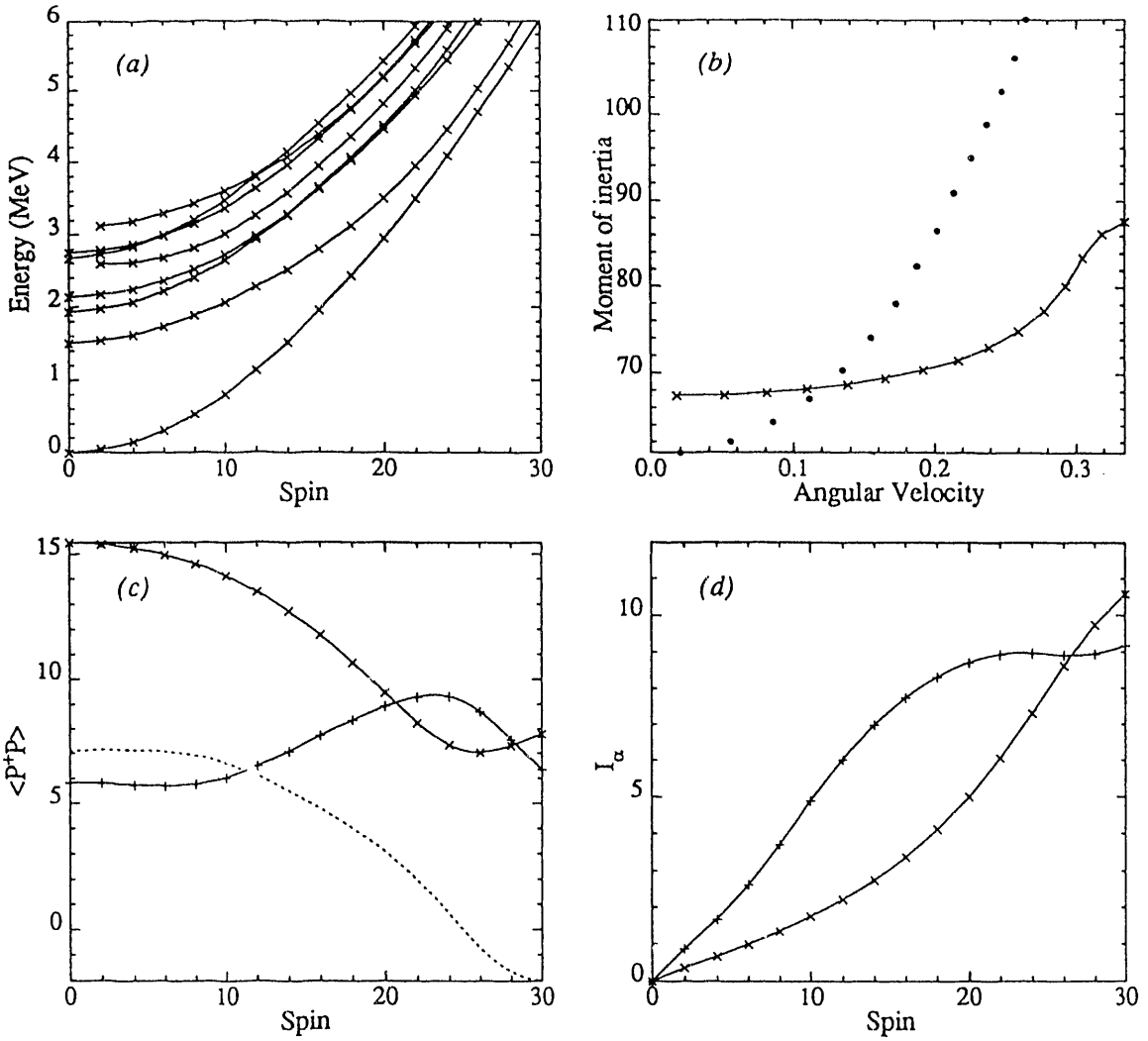

Figure 2: Same as Fig.1 except for ^{232}Th. Note in (c) the greater pairing vibration character of the yrare for spins up to 14 and in (d) its neutron-spin-aligned character at higher spins.

^{232}Th, and this results in qualitative differences among the subshell nucleus and its neighbors.

Note that nowhere in the level schemes does an idealized aligned band appear with energy minimum at a spin equal to the aligned angular momentum. The bandheads are always at the lowest spin in the band, unlike the aligned bands from angular-momentum-projected uncranked UHFB solutions of Y. Sun *et al.*[16] Rather in the HMD method the "aligned band" seems to be a kind of strength function that concentrates on different real bands in different regions of spin. Just below bandcrossing the yrare band has most of the aligned band character, as the large plateaus of aligned spin in Figs.1d and 2d show. For ^{234}Th in Fig.3 the situation is more complicated, with two bands competing for yrare. The comparisons with experimental data in

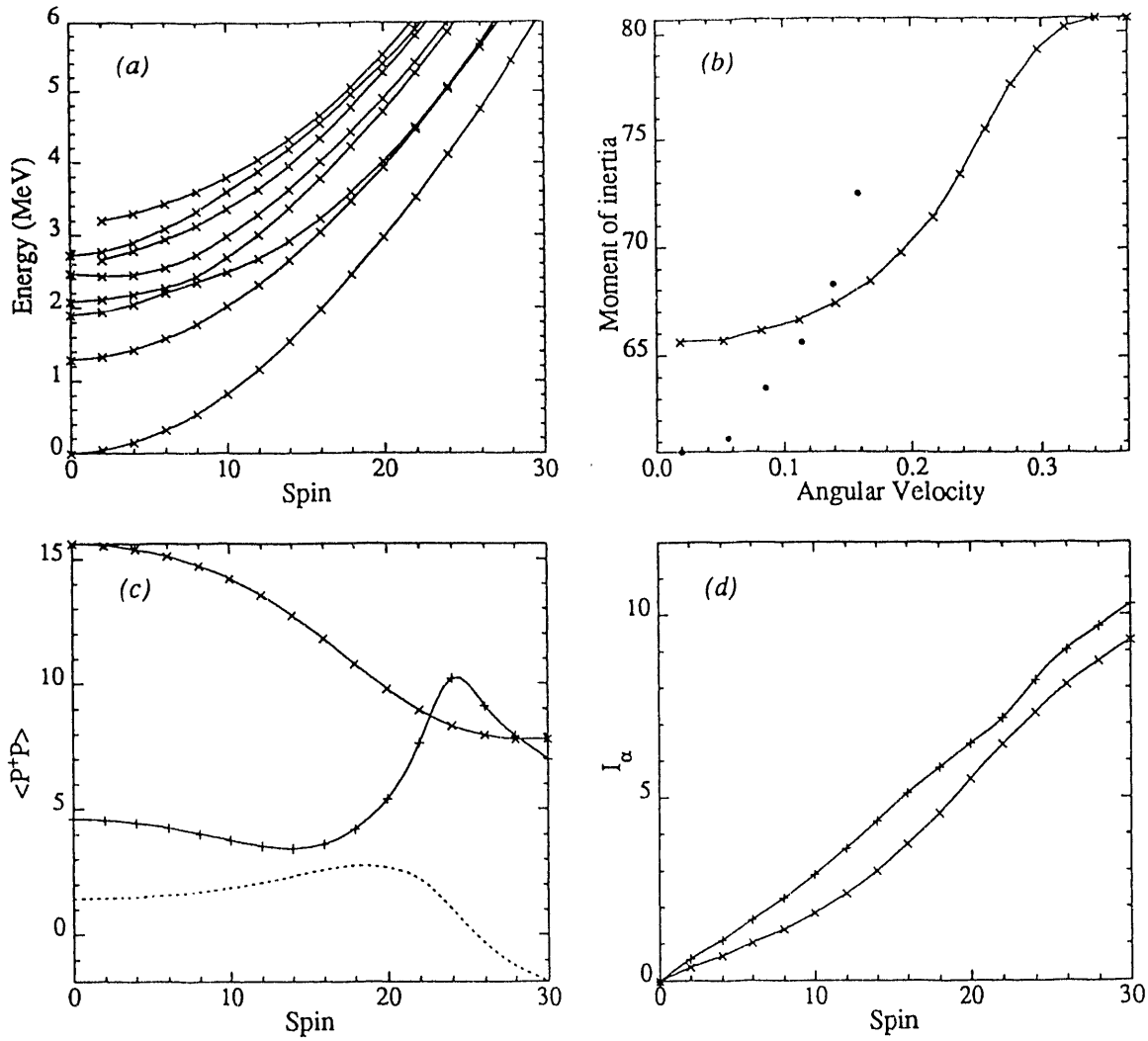

Figure 3: Same as Figs.1 and 2 except for ^{234}Th. Note in (c) that pairing vibration character of the yrare is small throughout.

the backbending plots do not seem very good, but we reiterate that the backbending plot is extremely sensitive to small shifts in single-particle energy levels. Furthermore, the Figs.1-3 calculations are exclusively for neutron systems to facilitate the HMD comparisons with CHFB+RPA, and it is well-known that proton alignment occurs for thorium in the same spin region as neutron alignment. The complementary model we will use here use a self-consistent cranked Hartree-Fock-Bogoliubov plus Random-Phase Approximation (CHFB+RPA) spanning a much larger shell-model space than HMD. The CHFB+RPA calculations were carried out by methods described in refs[9,10]. The energies of CHFB+RPA solutions are seen in Figs.4b and 5b, to be discussed in the next section on pair transfer strengths. The Coriolis Anti-Pairing in the CHFB calculation leads to static pairing collapse at a critical value of

$\hbar\omega_c = 0.20$ MeV (about $I = 18$). Above this $\hbar\omega_c$ only the dynamic RPA pairing correlations remain. Near the end of this paper we show a calculation of HMD coupling the neutron and proton systems. There we shall also show an idealized example of a bunched single-particle level set, where structural features are more prominent, but first we want to explore the pair-transfer strength distributions.

3. Pair-Transfer Strength Distributions

As mentioned in the introduction, the neutron-pair transfer properties connecting adjacent even-even isotopes have much intrinsic interest. The general yrast-to-yrast enhancement by the pairing force has been measured and studied a great deal. The conditions under which pair transfer strength may partially attach to excited bands are less understood. Some cases attributed to shape coexistence have been proposed[22]. Some tendency for strength to excited bands has been associated with gaps in the single-particle level spacing, leading to concentrations of pairing vibrational strength on excited bands. Some twenty years ago the principles of pair transfer strength in regions of bunched levels near closed shells or subshells[23] were elucidated. Recently C.Y. Wu *et al.*,[24] reviewed the subject of pairing correlations and pair transfer between heavy nuclei, where excitation to high spin states is extensive.

We realize that pair transfer need not be confined to transfer of pairs coupled to total angular momentum or even body-projected angular momentum zero. However, for this work we restrict ourselves, as do most such transfer studies, to this limit. We take the pair transfer operator of form $a^\dagger a^\dagger$ for addition of a pair and $a\,a$ for removal of a pair. In the case of the CHFB+RPA calculations here we just take the expectation value of these operators between yrast and excited states at various

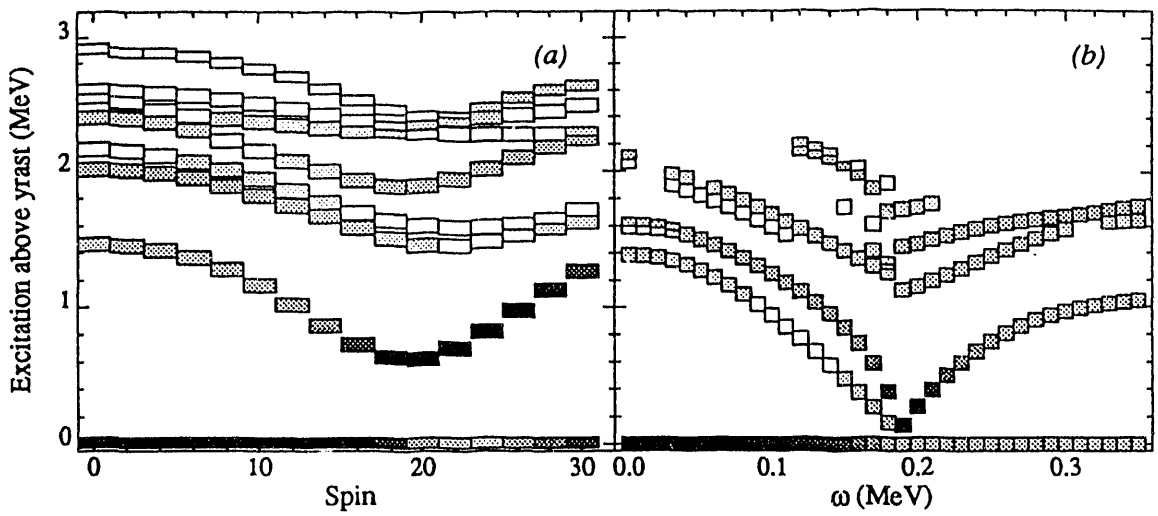

Figure 4: Gray-scale plots of neutron pair transfer strengths ($I \rightarrow I$ transitions) from yrast levels. (*a*) using HMD microscopic eigenvectors and (*b*) using CHFB+RPA methods. The reaction is neutron-pair removal from ^{232}Th.

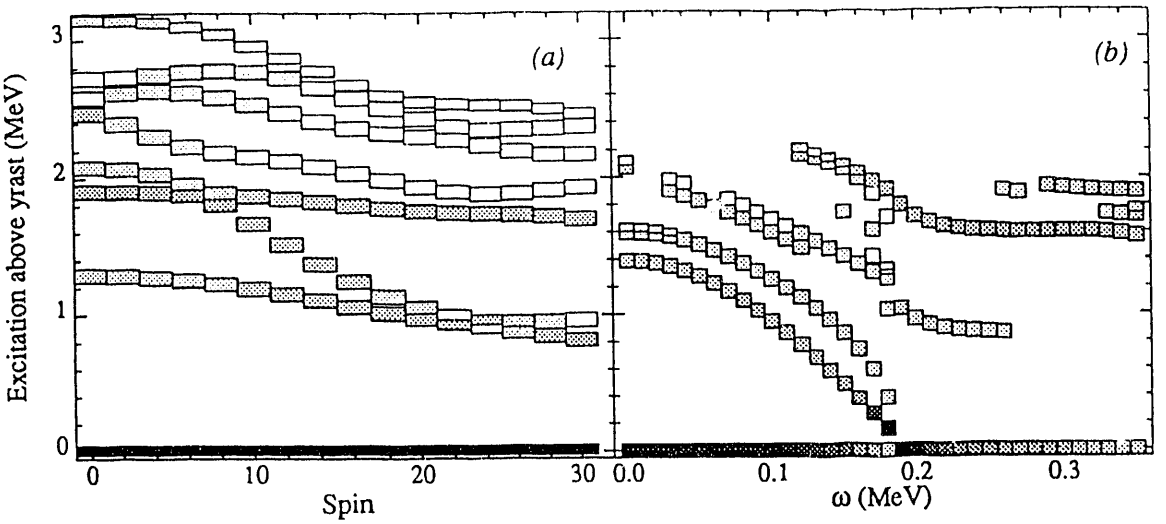

Figure 5: Same as Fig.4 except for neutron-pair addition to ^{232}Th.

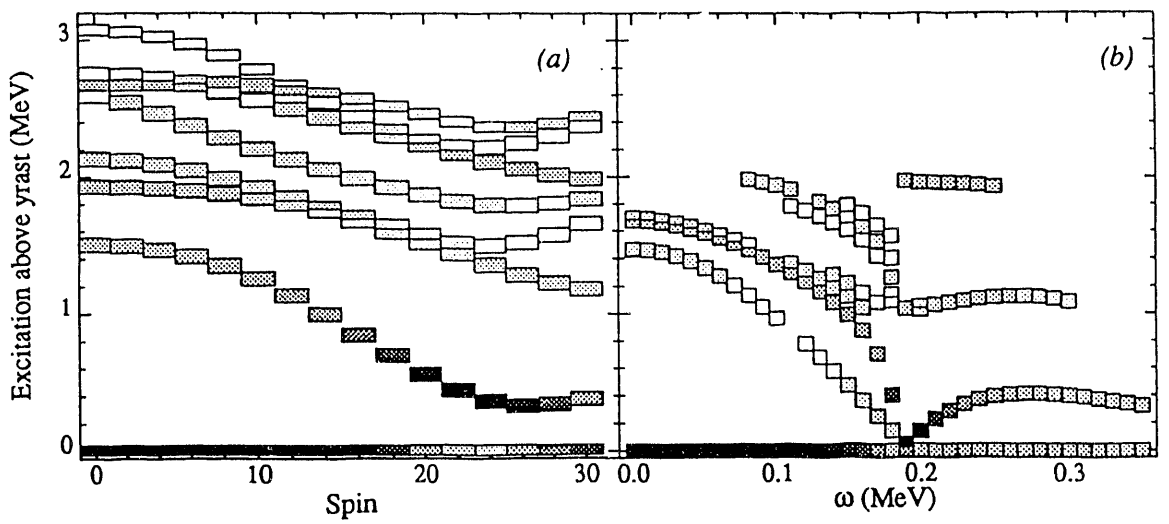

Figure 6: Same as Figs.4 and 5 except for neutron-pair addition to ^{230}Th.

values of the angular velocity ω. In the case of our microscopic HMD calculations we use the operators with appropriate $< A+2|$ or $< A-2|$ and $|A>$ states, respectively. For the HMD we take these pair-transfer amplitudes here between yrast level of given spin I in the initial nucleus and the first eight levels of that I in the final nucleus. The pairing strengths and level energies can be examined for patterns in the gray-scale plots of Figs.4-6 *a* and *b*. The *a* parts show the HMD calculations, and the *b* parts show the CHFB+RPA. In the latter there is a discontinuity at the critical angular velocity where static pairing vanishes. Below this critical value the RPA calculations bring in the pairing fluctuations about a static pairing vacuum state, and above the critical value the pairing fluctuations are about a zero-pairing vacuum

state. Figs.4 are for pair removal from ^{232}Th. For both methods we see at lower spin that the predominant transfer strength is in the yrast-to-yrast. Both methods show some strength settling in three places among the excited states between 1.5 and 2.5 MeV at lowest spins; the energies of these excited bands move down toward a cusp, then up with increasing spin and the transfer strength may shift between bands. The strength to excited states generally remains in three, sometimes four, solutions. Very close-lying excited states may have greatly differing transfer strengths. The apparent sporadic discontinuities in CHFB+RPA bands are because solutions with too low transfer strength were not saved. The discontinuity at the pairing phase transitions result because of change of the vacuum, and the CHFB+RPA is not expected to be valid close to this point. In comparing results for the two models it must be borne in mind that the spin I and angular velocity ω are not linearly proportional to each other. From Fig.1*b* it can be seen that in the upbending region several successive spin values from 16 to 24 have almost the same value of ω of about 0.24. The aligned band near crossing will have a lower ω for a given spin than the ground band; indeed, each excited band will have its own correspondence between I and ω. One can see some similarities in patterns between the two models for the other transfers depicted in Figs.5 and 6. In Fig.5*a* a limitation on our particular HMD model is seen, in contrast with CHFB+RPA in Fig.5*b*. The HMD here does not have sufficient Coriolis AntiPairing at highest spins, since we do not allow broken pairs in any but the $j_{15/2}$ orbitals. Hence, the ground-to-ground transfer in the HMD remains strong even at the highest spins, whereas the CHFB+RPA falls off as it should.

Figs.5*a* and 6*a* show in the band crossing region that there is predominant transfer strength between yrast and yrare. This is a consequence of the band crossings in initial and final nuclei being at somewhat different spins.

4. Pair Transfer Cross Sections

To go beyond the calculation of transfer matrix elements and obtain theoretical cross sections to compare with data is a challenging task. The Alder, Winther, deBoer method[25] has been adapted to explore the "diabolic" Berry-phase interference effects, first taking into account just yrast bands[26] and later taking both yrast and yrare bands in a coupled-channel treatment[27]. The above semiclassical treatments were restricted to head-on collisions to simplify the computation. The inclusion of the second band clearly was important, making the diabolic interference effects smaller.

Now when we look at the distribution of transfer strength among the eight lowest bands, we may well surmise that inclusion of more than two bands is necessary. Certainly, if theory is to confront the calorimetric data of the "HK" plots, total energy *vs.* number of gamma rays (fold), obtained from 4π gamma detector arrays, these higher bands need to be taken into account.

For the actinides with their larger moments of inertia it is worth reconsidering the sudden approximation approach, in which the spheroidal nucleus does not appre-

ciably rotate during the collision time. In this limit important simplifications can be made in the treatment. Let us derive the necessary formulas.

5. Sudden Approximation Formulas

Let the wavefunction from the HMD calculation be expressed as follows:

$$| I, M, \alpha, N >= \mathcal{N}_I \sum_{\mu} \mathcal{D}^I_{MK}(\Omega)\, b_\mu(I, \alpha; K, N)\, \varphi^N_\mu \tag{9}$$

where normalization constant $\mathcal{N}_I = \sqrt{I + 1/2}/(2\pi)$, the φ^N_μ are the basis wavefunctions for configuration with index μ, and $b_\mu(I, \alpha; K, N)$ is its amplitude from the HMD calculation. Then the amplitude for transition from the ground state $|\, 0M0, N >$ to $|\, IM\alpha, N+2 >$ is given by

$$\begin{aligned}
&\mathcal{A}_{00,N\to I\alpha,N+2} \\
&= \sum_{I_1\alpha_1}\sum_{I_2\alpha_2} < IM\alpha, N+2 \,|\, \mathcal{U}^\dagger \,|\, I_1 M\alpha_2, N+2 > < I_2 M\alpha_2, N+2 \,|\, \mathrm{Tx} \,|\, I_1 M\alpha_1, N > \\
&\qquad\qquad \times < I_1 M\alpha_1, N \,|\, \mathcal{U} \,|\, 0M0, N > \\
&= \int \mathcal{N}_I \sum_{\mu} \mathcal{D}^I_{MK}{}^*(\Omega)\, \exp\Big(-\frac{i}{\hbar}\int_0^\infty V(\Omega, R(t))\, dt\Big) \sum_{I_1,\alpha_2} \mathcal{N}_{I_1} \mathcal{D}^{I_1}_{MK}(\Omega)\, d\Omega \\
&\quad b_\mu(I, \alpha; K, N+2)\, b_\mu(I_1, \alpha_2; K, N+2) \\
&\quad \sum_{\alpha_1}\sum_{\mu'_2\mu'_1} b_{\mu'_2}(I_1, \alpha_2; K, N+2)\, b_{\mu'_1}(I_1, \alpha_1, I_1; K, N) \; < \varphi^{N+2}_{\mu'_2} \,|\, \sum_{\nu} \mathbf{a}^\dagger_\nu \mathbf{a}^\dagger_{\bar{\nu}} \,|\, \varphi^N_{\mu'_1} > \\
&\quad \mathcal{N}_{I_1} \int \sum_{\mu_0} \mathcal{D}^{I_1}_{MK}{}^*(\Omega_2)\, \exp\Big(-\frac{i}{\hbar}\int_{-\infty}^0 V(\Omega_2, R(t))\, dt\Big)\, \mathcal{N}_0 \mathcal{D}^0_{00}(\Omega_2)\, d\Omega_2 \\
&\quad b_{\mu_0}(I_1, \alpha_1; 0, N)\, b_{\mu_0}(0, 0; 0, N)
\end{aligned} \tag{10}$$

Let us define some auxiliary matrices.

- The matrix $\mathbf{X}^N_K(I_1, \alpha_1; I_2, \alpha_2)$ is the K component of the overlap of the intrinsic wavefunctions between two states with (I_1, α_1) and (I_2, α_2) in the nucleus of N neutrons. We can view this matrix $\mathbf{X}$ as a projection of the microstructure wavefunction, from eigenstate (I_1, α_1) to eigenstate (I_2, α_2).

$$\mathbf{X}^N_K(I_1, \alpha_1; I_2, \alpha_2) = \sum_{\mu} b_\mu(I_1, \alpha_1; K', N)\, b_\mu(I_2, \alpha_2; K', N) \delta_{K',K} \tag{11}$$

- The transition matrix $\mathbf{Y}^{N\to N+2}_I(\alpha_1, \alpha_2)$ is the overlap of intrinsic wavefunction before (in excitation state α_1) and after 2n transfer (in excitation state α_2) at spin I.

$$\mathbf{Y}^{N\to N\pm 2}_I(\alpha_1; \alpha_2) =$$

$$\sum_{\mu_1,\mu_2} b_{\mu_1}(I,\alpha_1;K_1,N)\, b_{\mu_2}(I,\alpha_2;K_2,N\pm 2)$$
$$\times < \varphi_{\mu_2}^{N\pm 2} \mid \sum_{\nu} \mathbf{a}_{\nu}^{\dagger}\mathbf{a}_{\bar{\nu}}^{\dagger} + \mathbf{a}_{\bar{\nu}}\mathbf{a}_{\nu} \mid \varphi_{\mu_1}^{N} > \qquad (12)$$

- The Coulomb excitation matrix $\mathbf{Z}_I$,

$$\begin{aligned}\mathbf{Z}_I &= \int \mathcal{D}^I_{00}(\Omega)\, \exp\Big(-\frac{i}{\hbar}\int_{-\infty}^{0} V(\Omega,R(t))\,dt\Big)\, d\Omega \\ &= \int \mathcal{D}^I_{00}(\Omega)\, \exp\Big(-\frac{i}{\hbar}\int_{0}^{\infty} V(\Omega,R(t))\,dt\Big)\, d\Omega \qquad (13)\end{aligned}$$

which is the component of the Coulomb excitation in spin I at closest approach.

Now the transfer matrix elements can be expressed in a more compact form as follows:

$$\mathcal{A}_{I_0\alpha_0,N\to I\alpha,N\pm 2} = \mathcal{N}_{I_0}\mathcal{N}_I \sum_{I_1,I_2,I_3} \mathcal{N}_{I_1}^2 (2I_2+1)(2I_3+1)\,\mathbf{Z}_{I_2}\mathbf{Z}_{I_3} \sum_{K_0,K}$$
$$\begin{pmatrix} I_0 & I_1 & I_2 \\ -M & M & 0 \end{pmatrix}\begin{pmatrix} I_0 & I_1 & I_2 \\ -K_0 & K_0 & 0 \end{pmatrix}\begin{pmatrix} I & I_1 & I_3 \\ -M & M & 0 \end{pmatrix}\begin{pmatrix} I & I_1 & I_3 \\ -K & K & 0 \end{pmatrix}$$
$$\sum_{\alpha_1,\alpha_2} \mathbf{X}^N_{K_0}(I_0,\alpha_0;I_1,\alpha_1)\,\mathbf{Y}^{N\to N\pm 2}_{I_1}(\alpha_1;\alpha_2)\,\mathbf{X}^{N\pm 2}_{K}(I_1,\alpha_2;I,\alpha) \qquad (14)$$

In particular, if the initial state is the zero spin ground state, then

$$\mathcal{A}_{00,N\to I\alpha,N\pm 2} =$$
$$\mathcal{N}_0\mathcal{N}_I \sum_{I_1} \mathcal{N}_{I_1}^2\,\mathbf{Z}_{I_1} \sum_{I_3}(2I_3+1)\mathbf{Z}_{I_3}\begin{pmatrix} I & I_1 & I_3 \\ 0 & 0 & 0 \end{pmatrix}\sum_{K}\begin{pmatrix} I & I_1 & I_3 \\ -K & K & 0 \end{pmatrix}$$
$$\times \sum_{\alpha_1} \mathbf{X}^N_0(0,0;I_1,\alpha_1)\sum_{\alpha_2}\mathbf{Y}^{N\to N\pm 2}_{I_1}(\alpha_1;\alpha_2)\,\mathbf{X}^{N\pm 2}_{K}(I_1,\alpha_2;I,\alpha) \qquad (15)$$

6. Transfer and Rotational Inelastic Probabilities

For the sample numerical calculations shown here we took the reaction ^{206}Pb on ^{232}Th at 1180 MeV (lab). The microscopic HMD wave functions are with the 12 Nilsson orbitals at the Bengtsson-Ragnarsson single-particle energies, as for our earlier figures. Space limitations preclude our showing also the calculations for a ^{90}Zr beam, but the heavier beam is considered of more interest, since it pumps rotational population into the band mixing region at closest approach. Figs.7*a-d* show the results. Fig.7*a* plots the yrast rotational state population at closest approach and before transfer. Fig.7*b* shows in gray scale the absolute value of the amplitudes in the various spin states of the lowest eight bands. We see the familiar oscillating

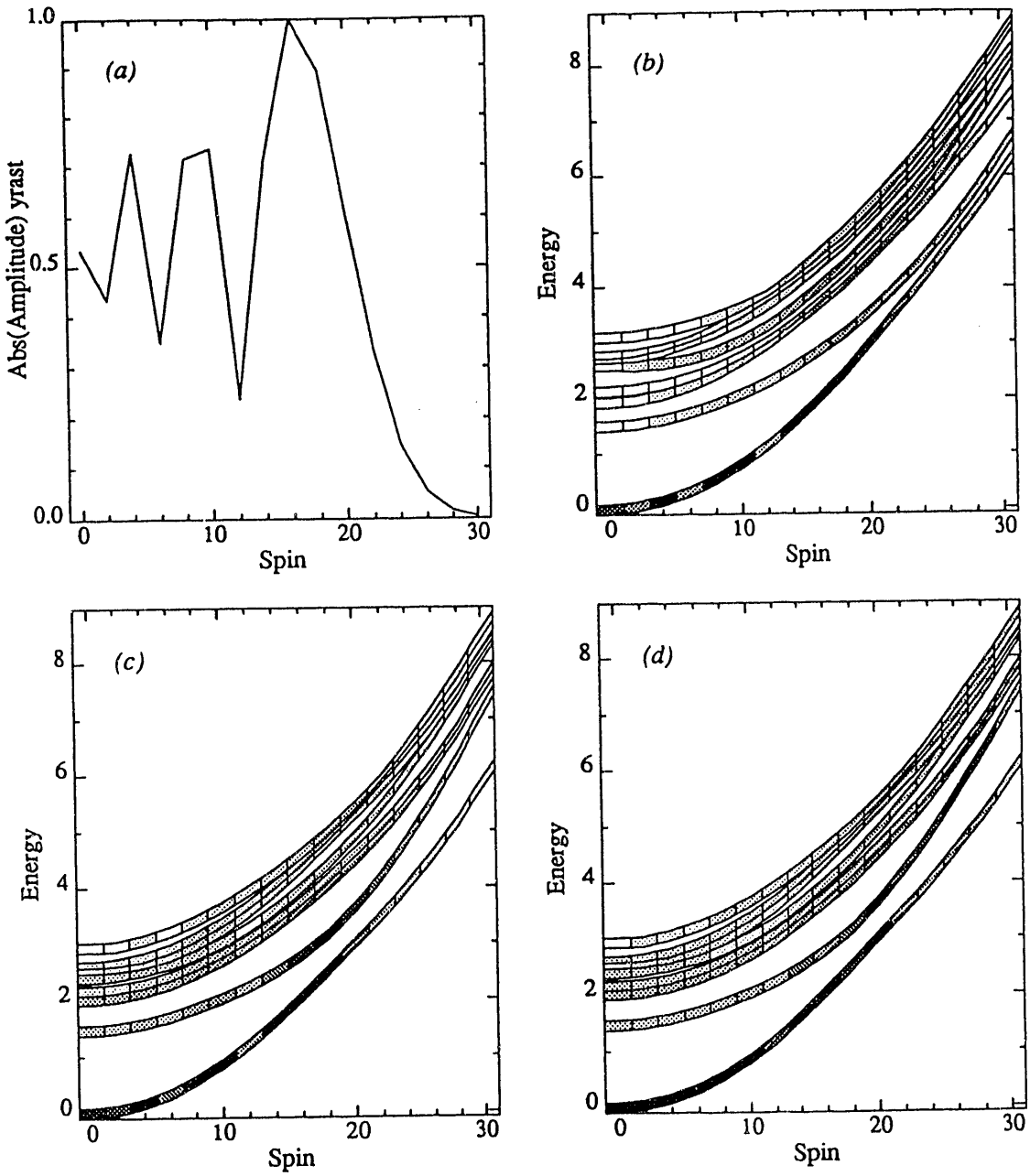

Figure 7: Theoretical HMD sudden-approximation amplitudes in reaction of ^{206}Pb +^{232} Th. (a) yrast band and (b) all-band population in ^{232}Th from Coulomb excitation at closest approach but before transfer. (c) population in ^{230}Th at closest approach immediately after pair transfer, and (d) population in ^{230}Th after collision partners have fully separated.

interference pattern dominated by a rainbow maximum at spins 16-18. There is a fair amount of population in the excited bands, a consequence of band-mixing. Fig.7c shows in gray scale the absolute values of the complex amplitudes immediately after the $I \rightarrow I$ transfer. It is evident that most population is still in the yrast band

with about the same spin distribution as before transfer. A considerable population is in the yrare band, peaking at spin 18, and some population is spread into all the other six higher bands. The transfer population to excited bands is enhanced by the Q-window centering at the Q value of 2 MeV. In excited bands the intensity oscillations with spin value seem nearly washed out compared to yrast. Fig.7*d* shows the final amplitudes after the collision partners have widely separated. There is further pumping of spin to higher values, the main population now being in the yrare band, which is the continuation of the ground band past spin 18, where the aligned band crosses under. There is good reason to distrust the sudden approximation in the final stage of Coulomb excitation on the outward path. The system of Pb + Dy was studied by Canto *et al.*,[26] using an Alder, Winther, deBoer semiclassical method, and spin populations were found to change very little on the outward path. The sudden approximation may be a little better for the actinide target, with its higher moment of inertia, but the final spin distribution may be something between those shown in Figs.7*c,d*.

7. Idealized Bunched Nilsson-level Case

It is instructive to repeat the above structure and transfer calculations for a case where the Nilsson levels nearest the chemical potential are bunched, rather than in the near-uniform distribution of the Bengtsson and Ragnarsson[21] values used above. Other calculations show something of a neutron subshell at ^{232}Th. To accentuate this tendency we carry out calculations where the odd-parity $j_{15/2}$ levels retain their BR values but the nearest three even-parity, lower-j orbitals are made nearly degenerate with the $5/2^-$ and with the $7/2^-$ level. Figs.8 and 9 show the structure calculation results for ^{230}Th and ^{232}Th, respectively. In the former case the chemical potential is within the cluster of four Nilsson levels around the 7/2−. The pairing force splits out a ground band with large pairing and leaves a nearly degenerate triplet of bands at 1.5 MeV, as simple considerations would lead one to expect. The very small off-diagonal pairing between yrast and yrare below spin 8 shows that the pairing correlation completely concentrates on the lowest level for the system of degenerate Nilsson orbitals, and there is no pairing vibrational character in the near-degenerate set of excited states. Above spin 8 the character of the yrare band changes to a spin-aligned band, which makes a sharp crossing with the ground band at spin 24. Fig.9 shows quite a different picture for ^{232}Th, the nucleus at the subshell. Band mixing is very diffuse, with yrast and yrare bands never getting very close. The eight Nilsson levels equidistant from the Fermi energy (four above and four below) give rise under the pairing force to a highly paired ground band and a moderately paired yrare band, increasing in pairing correlation with spin and exceeding the yrast in pairing by spin 16. The large off-diagonal pairing matrix element between yrast and yrare below spin 16 shows the pairing-vibrational nature of the yrare. Above the two collective bands is a cluster of 6 nearly degenerate bands. The blip in energy of the highest band at

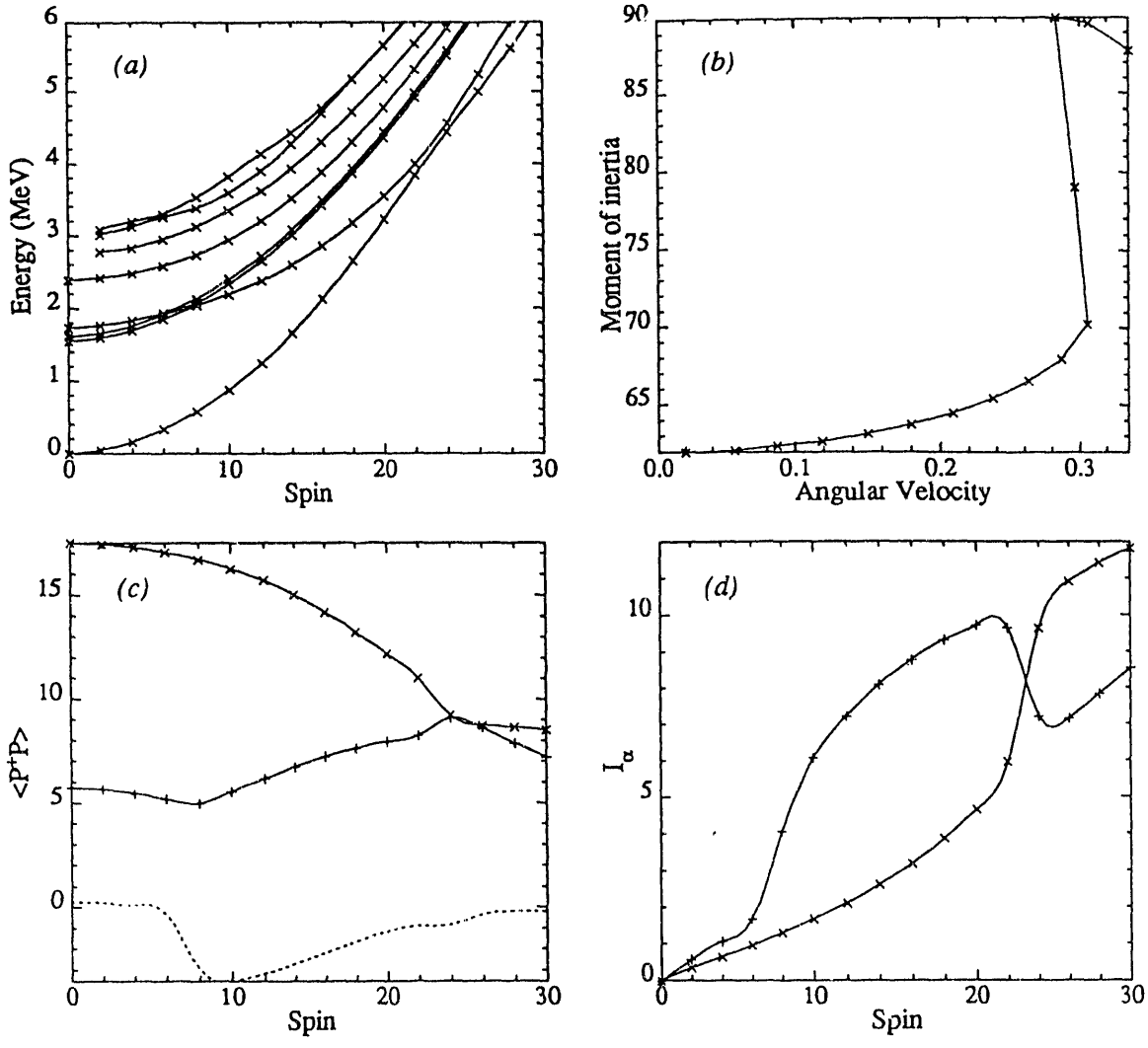

Figure 8: Same as Fig.1 (^{230}Th) except that Nilsson single particle levels have been artificially bunched into two bunches of four each on either side of the Fermi energy (see text and Table 1).

spin 10 probably shows that the Lanczos algorithm broke down and missed a state, where the degeneracy was high.

Figs.10*a,b* shows the $I \rightarrow I$ pair transfer matrix elements from yrast of ^{232}Th for this bunched-level idealized case. Fig.10*c* shows the corresponding values for ^{230}Th going into the subshell of ^{232}Th. The pattern is just what Bohr and Mottelson led us to expect in their early treatment of pairing vibration. That is, pair transfer out of the subshell (Fig.9) goes predominantly to ground, while transfer into the subshell (Fig.10) has a fair fraction of strength going to the first-excited pairing-vibrational state. Though we do not show a figure the calculations for 2n removal from ^{234}Th, going into the subshell from the other side show much the same pattern as Fig.10*c*.

The 1986 work of Egido and Rasmussen[28] on 2n transfer strengths in the Dy

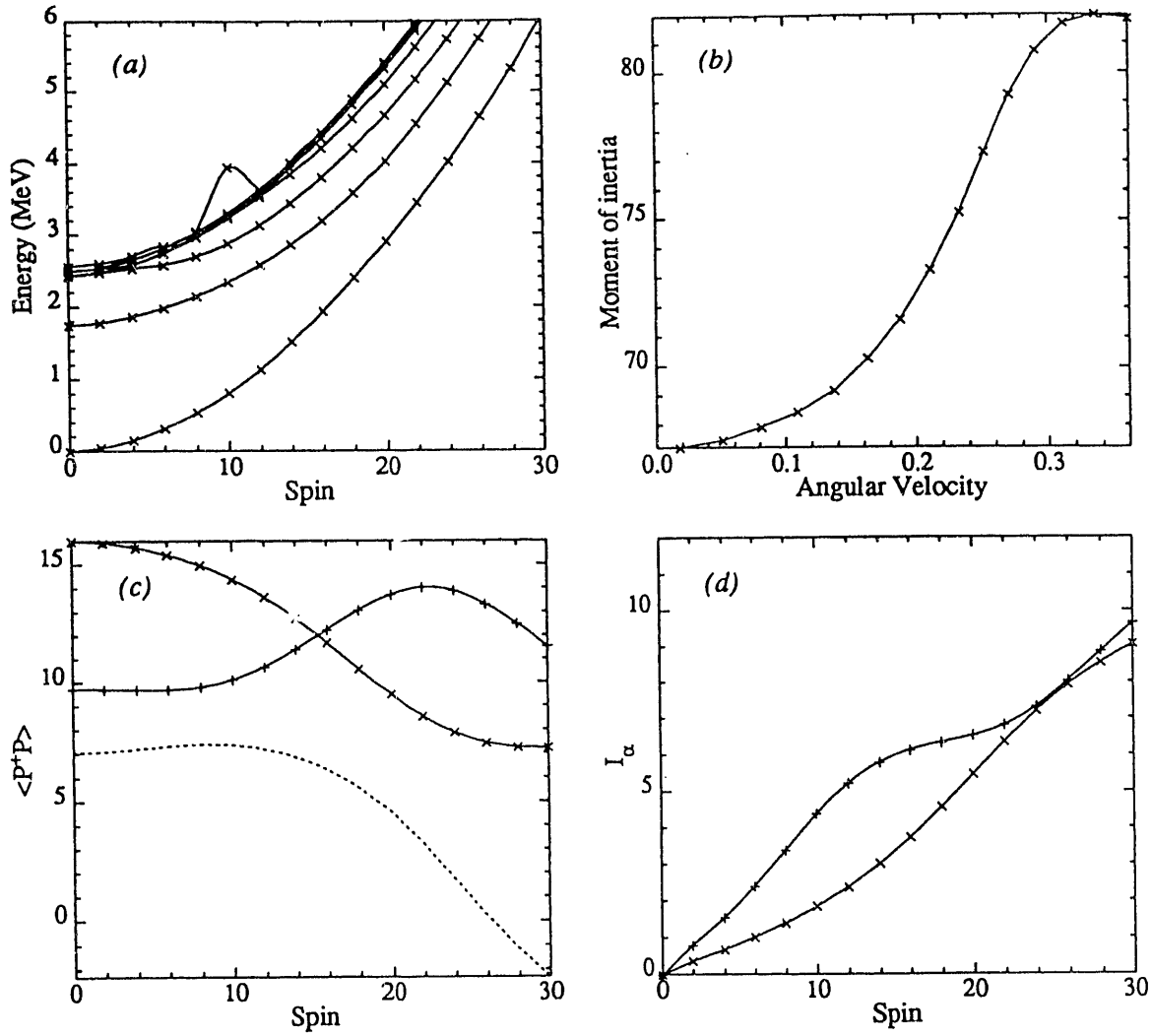

Figure 9: Same as Fig.8, except for ^{232}Th.

region showed a great deal of structure and fluctuation on up to the 10 MeV calculated. Only the strength to the yrast and yrare bands was systematically discussed. With insights from our new calculations we would suggest that 2n addition(removal) to(from) excited bands probes the non-uniformity of energy distribution of Nilsson levels above(below) the Fermi energy.

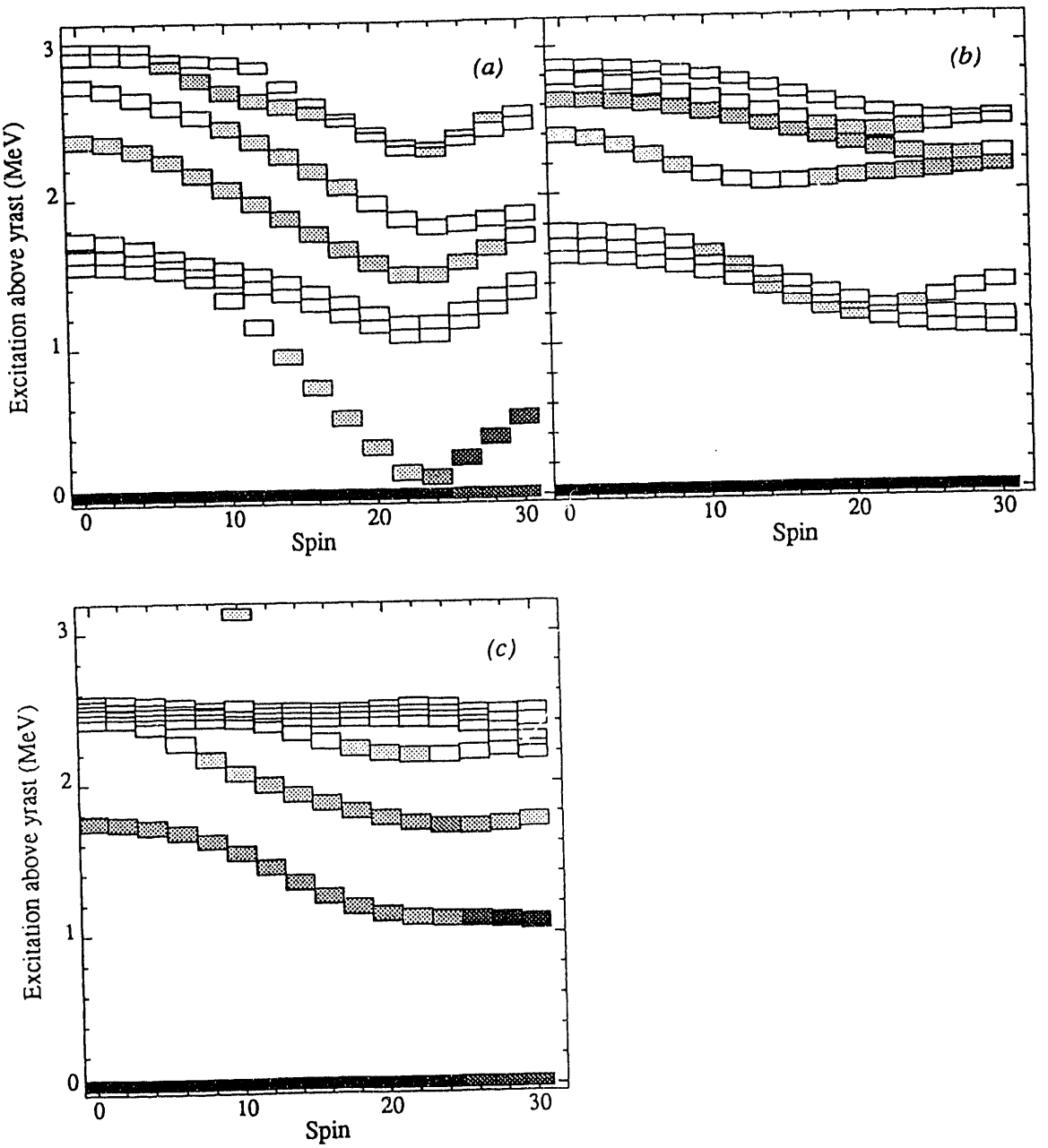

Figure 10: (*a*) Same as Fig.4*a* ^{232}Th $\rightarrow^{230}$ Th except using idealized level bunching as in Figs.8 and 9, (*b*) Same as Fig.5*a* ^{232}Th $\rightarrow^{234}$ Th. except using idealized level bunching. (*c*) Same as Fig.6*a*, ^{230}Th $\rightarrow^{232}$ Th, except using idealized level bunching.

8. Interconnection of Proton and Neutron Alignment

To avoid greatly complicating nuclear structure calculations in heavier nuclei, where neutrons and protons are filling different shells, a factorization is often assumed. That is, neutron structure and proton structure are independently calculated. For high-spin studies in the deformed rare earths that may be valid for many properties, since neutron alignment always occurs at lower spin values than proton alignment. For the actinide region, though, such factorization is less justified, since the protons and neutrons undergo spin alignment in the same region. As a final illustration of the potentialities of the HMD method with modern computers, we show two calculations on ^{232}Th. The first, shown in Fig.11, is as before, with neutron structure alone. We use 12 Nilsson orbitals but with orbital energies calculated with the SWGAMMA code of Nazarewicz for $\beta_2 = 0.208$ and $\beta_4 = 0.105$ from the tables of Moller and Nix. We use axial symmetry in the code SWGAMMA for Woods-Saxon potential. These energies are shown in the last column of Table 1. Our earlier comments about the sensitivity of sharpness of band crossing to the single particle level energies are further illustrated. Even though the single particle energies for Fig.11 are only slightly changed from the Bengtsson and Ragnarsson energies of Fig.1, we now see sharp band crossing in Fig.11*a*.

Finally we go to an HMD calculation combining a 9-Nilsson-level neutron system with a similar proton system. We do not add any explicit np force terms to the Hamiltonian, but n-p coupling arises not only in our recoil-energy term but also through the rotor-particle Coriolis coupling. Such effects are easy to see in the spin-alignment graphs of Egido and Ring[18], where one type of nucleon may begin gradually to align and the other suddenly aligns, with a concomitant decrease of alignment of the first type. The sudden alignment has slowed the rotor and decreased the alignment of the other type of nucleon.

Figs.12*a-f* show the results of the combined calculation. The dimensionality of the matrix has been decreased by an energy criterion that cuts out the less important configurations. Even so, the Hamiltonian matrix here has dimensionality of 19,098. The matrix is rather sparse, with 275,189 non-vanishing matrix elements. Parts of the code with the Lanczos algorithm require quadruple precision in the Sparcstations and double precision on the U.C Berkeley Cray in order to converge. The eight lowest roots were taken for the 16 diagonalizations at the 16 different spin values. The CPU time on the Sparcstation ELC was 73 hrs.

Note the differences between the pure neutron and the grand combined calculations. The sharp backbending at spin 18-20 in the neutron case shift to spin 22 in the coupled case. From Figs.12*c,d* we see that the first two excited bands at spin 0-4 are neutron excitations and factorization is perfect, since the proton pairing is unchanged. From Figs.12*e,f* it is evident that for intermediate spins 10-16 the first excited band has neutron alignment character and the second excited band proton alignment. Figs.12*c,d* show that the aligned bands have a low degree of pairing in the type of nucleon that is aligned. Fig.13 shows the corresponding plots for the grand

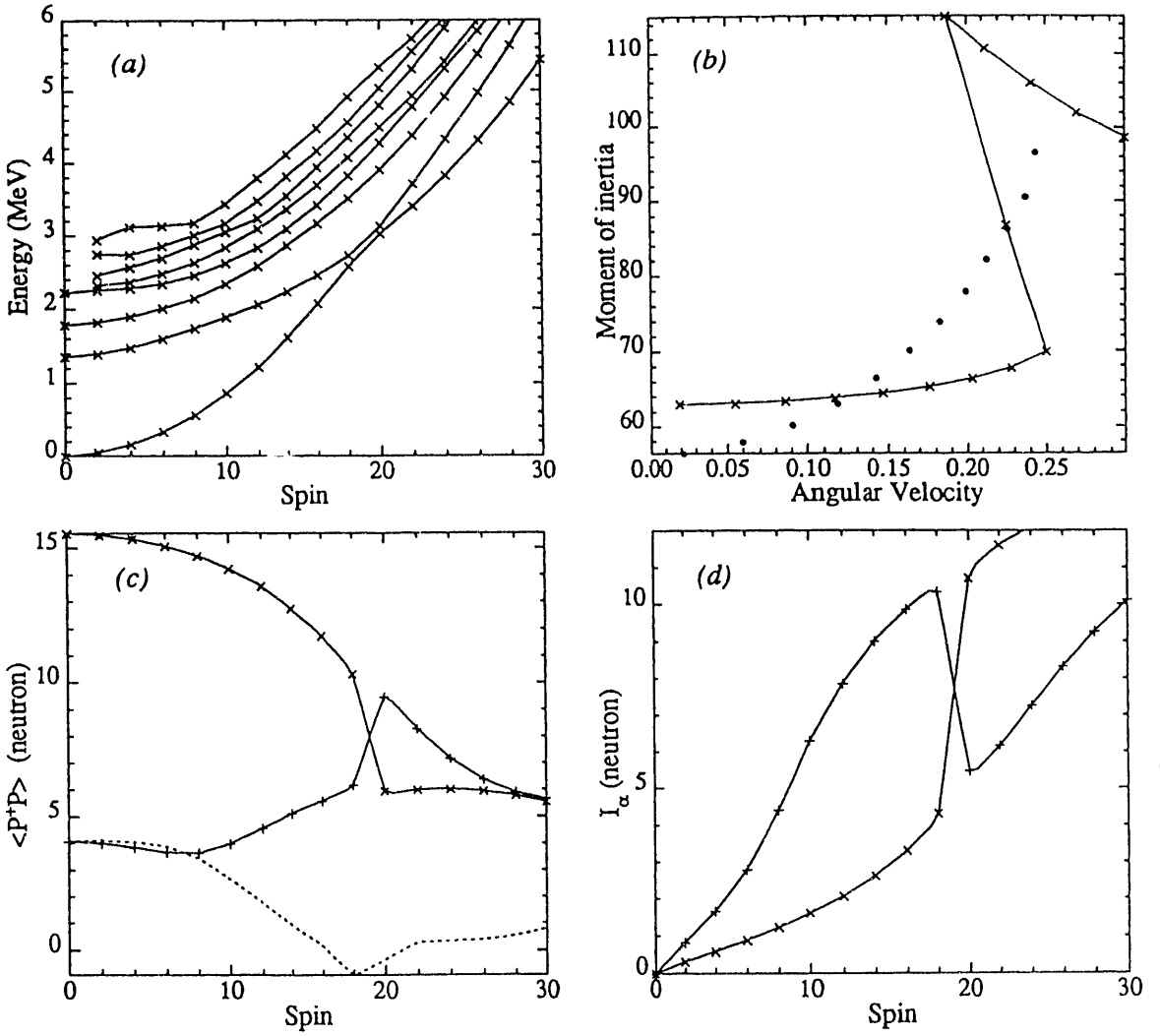

Figure 11: Same as Fig.1 for ^{230}Th except with Nazarewicz-code for the 12 Nilsson energies instead of Bengtsson and Ragnarsson energies (see Table 1.)

combined calculation on ^{232}Th. Beyond a crossing of excited bands at spin 8 the yrare band is mainly a proton-alignment bands. The neutron spin alignment does not as cleanly concentrate on a single band.

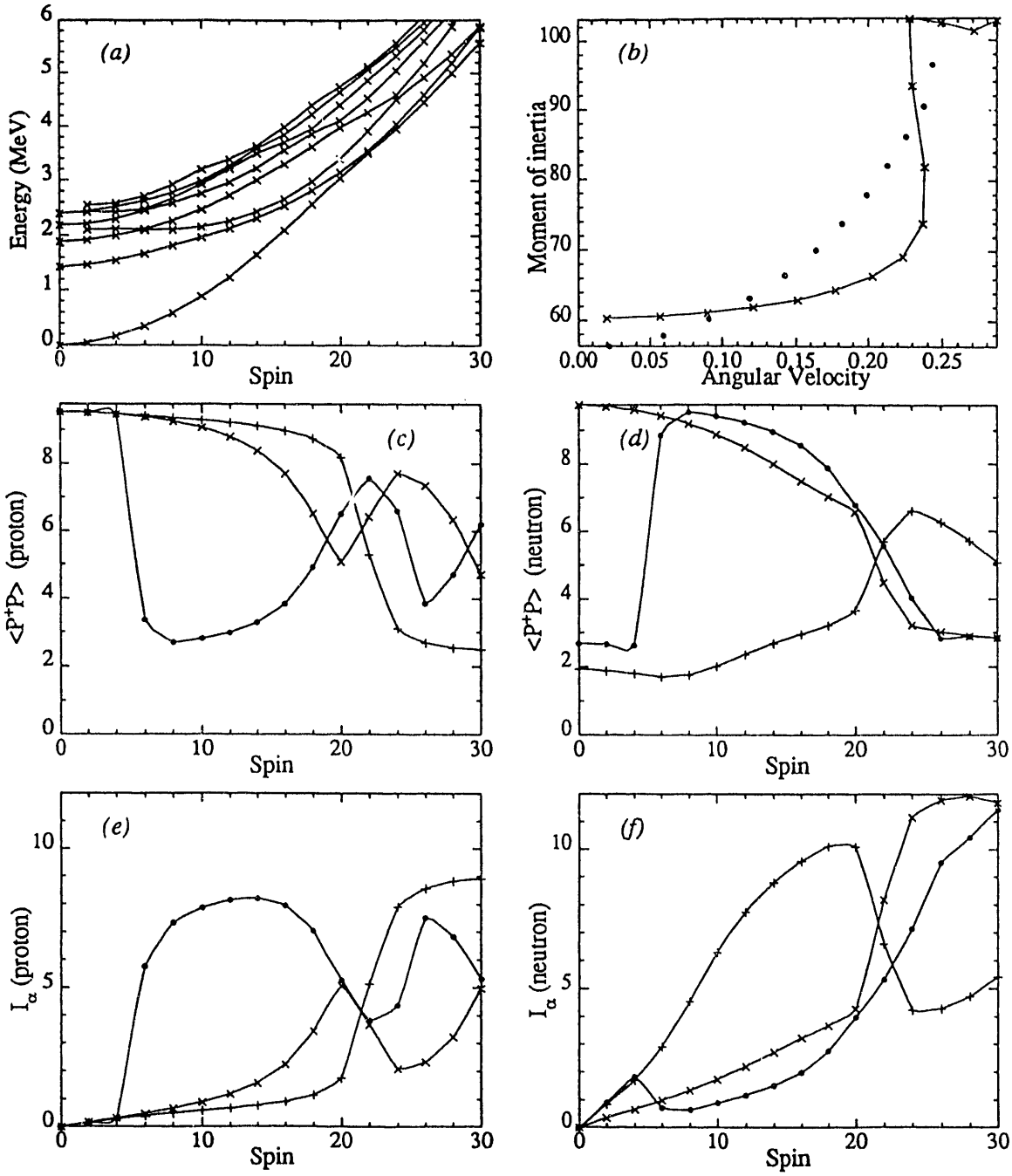

Figure 12: Grand combined HMD calculation for ^{230}Th with 9 neutron and 9 proton Nilsson orbitals and Nazarewicz energies (see Tables 1,2). This is like Fig.1 except that proton as well as neutron-alignment and pairing is shown and for the lowest three bands, yrast(×), yrare(+), and second-excited(•).

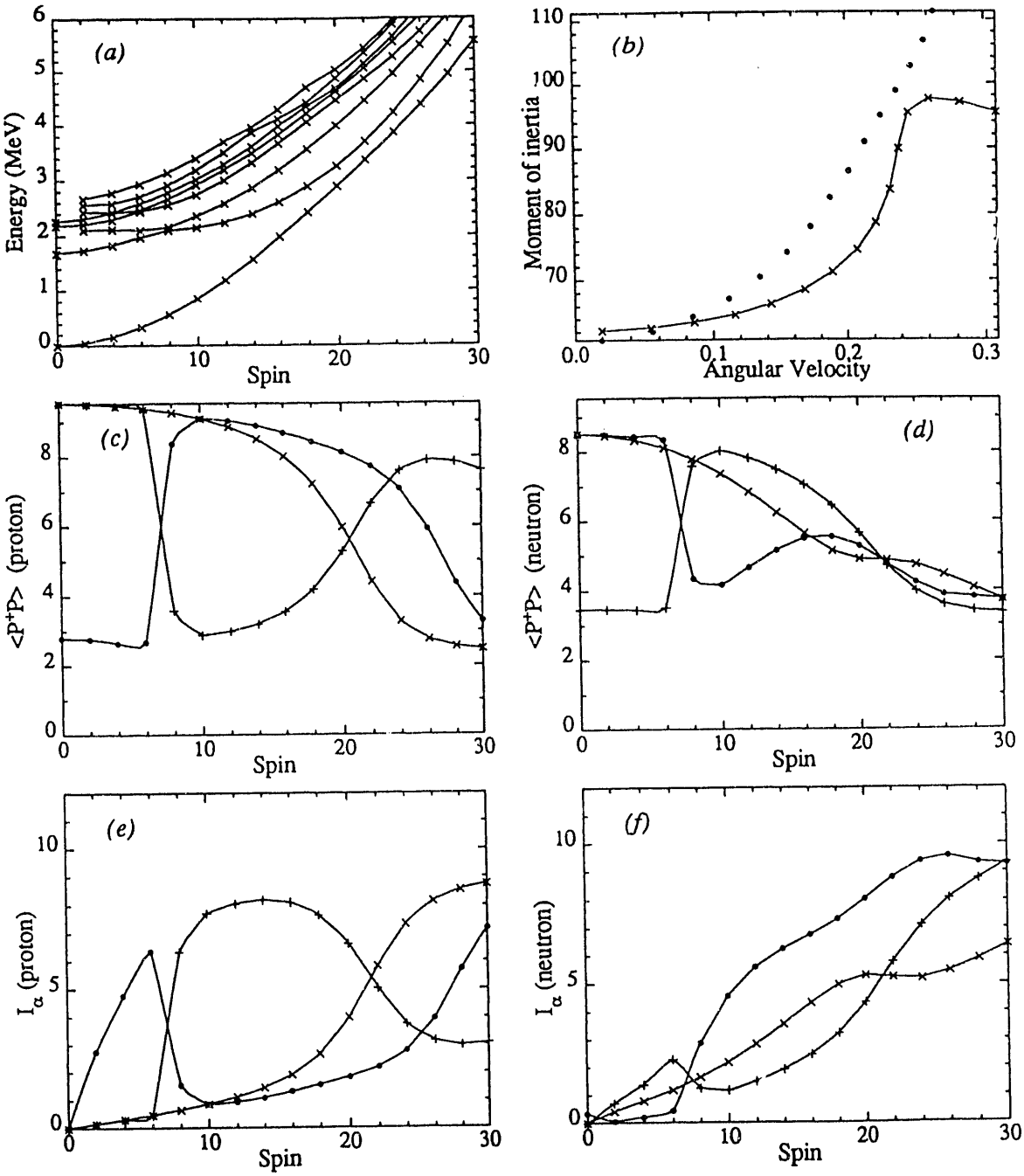

Figure 13: Same as Fig.12 except for ^{232}Th.

9. Conclusion

We have presented here some samples of what can be done on nuclear rotational band theory with high-speed desktop computers. By straightforward Hamiltonian matrix diagonalization (HMD) we calculate families of $K = 0^+, 1^+$, and 2^+ bands in spheroidal even-even nuclei, obtaining wave functions conserving particle number and total angular momentum. With such wavefunctions, band mixing behavior can readily be studied through spin alignment and pairing properties of various states.

Quadrupole pairing and quadrupole-quadrupole field terms in the Hamiltonian were turned off in the actinide calculations shown here, since we wished to make direct comparisons between HMD and CHFB+RPA calculations for neutron-pair transfer. Comparing the two approaches we find remarkably similar patterns in the transfer strength distributions. This gives us some confidence that the similar patterns may be realistic, and with the two methods, one may guess the results in those regions, where each of the approaches is weakest (HMD at high spin, where the CAP is strong and CHFB+RPA near the transition point). The measurable population pattern is very much dominated by the COULEX. Thus, to study the transfer pattern experimentally one needs to study the impact energy and scattering angle dependence carefully, to disentangle, as far as possible, the COULEX pattern from the transfer pattern.

We made exploratory studies of quadrupole pairing in the 90-neutron region, and we note its importance in lowering the pairing vibrational band head. This influence of downsloping (polar) and upsloping (equatorial) Nilsson orbitals near the Fermi surface, and the region of thorium nuclei studied in this paper should be less sensitive to quadrupole pairing.

Our HMD calculations to date have been constrained to fixed deformation, a reasonable constraint for ^{232}Th and its neighboring isotopes. However, if HMD is to be extended to the very borders of stable deformation or into some of the sub rare-earth regions with shape coexistence pioneered by Joe Hamilton and associates, we must develop a measure of self-consistency in shape determination. It seems promising to add quadrupole-quadrupole field interactions among the valence nucleons in the 9-12 Nilsson orbitals, thus, opening the approach to shape self-consistency and shape coexistence phenomena.

10. Acknowledgments

This work was mainly supported at Lawrence Berkeley Laboratory by the Director of Energy Research, Division of Nuclear Physics of the Office of High Energy and Nuclear Physics of the U.S. Department of Energy under contracts DE-FG03-87ER40323 and DE-AC03-76SF00098. J.O.R. wishes to acknowledge the Alexander von Humboldt Foundation for support of three months of work at the Technical University of Munich in Garching, and he greatly benefited from discussions with P. Ring, Y. Sun, K. Hara, H.J. Mang, and J. L. Egido. R.D. gratefully acknowledges travel support for a month in Berkeley from the Brazilian-Conselho Nacional de Pesquisas

e Desenvolvimento Cientifico (CNPq) under U.S.-Brazil NSF-CNPq cooperative research grant INT-8382853. S.F. and R.D. acknowledge hospitality and support of Nuclear Science Division, LBL. during their recent stays.

11. References

1. O. Nathan and S. G. Nilsson in Siegbahn, *Alpha, Beta, and Gamma Spectroscopy,* (1965) p.601.
2. J. Gerl, W. Korten, D. Habs, D. Schwalm, and H. J. Wollersheim, *Z. Phys.* **A334** (1989) 195;
   H. J. Wollersheim, Th. W. Elze, and K. Stelzer, *GSI Darmstadt Annual Report* 92-1 (1992) p.15;
   G. Eckert, K. Stelzer, R. O. Nelson, T. W. Elze, et al., *Z. Phys.* **A343** (1992) 267.
3. A. Bohr and B. R. Mottelson, *Nuclear Structure* Vol.2 (Benjamin, Reading, MA, 1975) p.646.
4. M. W. Guidry, T. L. Nichols, R. E. Neese, *et al.*, *Nucl. Phys.* **A361** (1981) 274.
5. A. Johnson, H. Ryde and J. Sztarkier, *Phys. Lett.* **B34** (1971) 605;
   A. Johnson, H. Ryde and S. A. Hjorth, *Phys. Lett.* **A179** (1972) 753.
6. F. S. Stephens and R. S. Simon, *Nucl. Phys.* **A183** (1972) 257.
7. R. S. Nikam, P. Ring and L. F. Canto, *Z. Phys.* **A324** (1986) 241;
   R. S. Nikam, P. Ring and L. F. Canto, *Phys. Lett.* **B165** (1987) 269;
   C. H. Dasso, A. Winther, *Phys. Lett.* **B242** (1990) 323.
8. R. Bengtsson, I. Hamamoto, B. Mottelson, *Phys. Lett.* **B73** (1978) 259.
9. R. Broglia, M. Diebel, S. Frauendorf, and M. Gallardo, *Phys. Lett.* **B166** (1986) 252.
10. Y. R. Shimizu, J. D. Garrett, R. A. Broglia, M. Gallardo, and E. Vigezzi, *Revs. Mod. Phys.* **61** (1989) 131.
11. T. Engeland, *Proc. Nordic Winter School on Nuclear Physics (April 1983)* (World Scientific, Singapore, 1984) p. 155.
12. B. A. Brown, in *Proceedings of the Workshop on Microscopic Models in Nuclear Structure Physics, Oak Ridge Oct 3-6, 1988* (World Scientific, Singapore, 1989) p.337.
13. H. J. Mang, J. O. Rasmussen and M. Rho, *Phys. Rev.* **141** (1966) 941.
14. S. Y. Chu, E. R. Marshalek, P. Ring, J. Krumlinde, and J. O. Rasmussen, *Phys. Rev.* **C12** (1975) 1017.

15. A. A. Shihab-Eldin, J. O. Rasmussen and M. Stoyer, *Proceedings of the Workshop on Microscopic Models in Nuclear Structure Physics, Oak Ridge Oct 3-6, 1988* (World Scientific, Singapore, 1989) p.282.

16. K. Hara and Y. Sun, *Z. Phys.* **A339** (1991) 15;
cf. also Y. Sun, Doctoral thesis, Tech. Univ. Muenchen (1991) (unpublished).

17. M. S. Rhoades-Browne, R. Donangelo, M. W. Guidry, and R. E.Neese, *Phys. Rev.* **C24** (1981) 2747.

18. J. L. Egido and P. Ring, *Nucl. Phys.* **A423** (1984) 93.

19. Y. R. Shimizu and S. Frauendorf, (unpublished) (1992).

20. Original Lanczos code provided courtesy of Prof. B. H. Wildenthal.

21. T. Bengtsson and I. Ragnarsson, *Nucl. Phys.* **A436** (1985) 14.

22. P. Debenham and N. M. Hintz, *Nucl. Phys.* **A195** (1972) 385;
also see the review article R. A.Broglia, O. Hansen and C. Riedel, *Adv. Nucl. Phys.* **6** (1973) 287.

23. A. Bohr and B. R. Mottelson, *Nuclear Structure*, volume II (1975) (W. A. Benjamin, Inc.) p.646.

24. C. Y. Wu, W. von Oertzen, D. Cline, and M. W. Guidry, *Ann. Rev. Nucl. Part. Sci.* **40**, (1990) 285.

25. K. Alder and A. Winther, *Electromagnetic Excitation,* (North-Holland, 1975).

26. L. F. Canto, R. Donangelo, M. W. Guidry, A. R. Farhan, J. O. Rasmussen, P. Ring and M. A. Stoyer, *Phys. Lett.* **B241** (1990) 295.

27. C. H. Dasso and A. Winther, *Phys. Lett.* **B242** (1990) 323;
L. F. Canto *et al.*, (submitted to *Phys. Rev. C*).

28. J. L. Egido and J. O. Rasmussen, *Phys. Rev.* **C36** (1987) 316.

END

DATE FILMED

5/21/93